Measurement of Normal and Anomalous Diffusion of Dyes within Protein Structures Fabricated via Multiphoton Excited Cross-Linking

Swarna Basu,† Charles W. Wolgemuth, and Paul J. Campagnola*

University of Connecticut Health Center,
Department of Cell Biology and Center for Cellular Analysis and Modelling,
Farmington, Connecticut 06030

Received May 17, 2004; Revised Manuscript Received July 2, 2004

We demonstrate microscale spatial and chemical control of diffusion within protein matrixes created through the use of nonlinear multiphoton excited photochemistry. The mobility of fluorescent dyes of different mass and composition within controlled cross-linked environments has been measured using two-photon excited fluorescence recovery after photobleaching (FRAP). The diffusion times for several rhodamine and sulforhodamine dyes within these fabricated structures were found to be approximately 3−4 orders of magnitude slower than in free solution. The precise diffusion times can be tuned by varying the laser exposure during the fabrication of the matrix, and the diffusion can be correlated with the mesh size determined by TEM and Flory−Rehner analysis. We find that the hydrophobic Texas Red dyes (sulforhodamines) exhibit diffusion that is highly anomalous, indicative of a strong interaction with the hydrophobic cross-linked protein matrix. These results suggests the use of these cross-linked protein matrixes as ideal model systems in which to systematically study anomalous diffusion. Finally, the diffusion can be tuned within a multilayered protein matrix, and this in conjunction with slow diffusion also suggests the use of these structures in controlled release applications.

Introduction

The ability to exert regional and chemical control on diffusion properties within micron-scale cross-linked protein matrixes has several important fabrication applications in biomedical fields. For example, experiments designed to measure and control diffusion can provide vital information for the development of devices for highly localized sustained release and drug delivery. Other areas of importance include tissue engineering (e.g., directed cell growth on extra-cellular matrixes and cell encapsulation for in vivo repair) and microfluidics relevant to chip-based assays. Although a great deal of work has investigated the diffusion of macromolecules and macromolecule-sized dye-dextrans in solution[1−4] our approach is to study the entrapment and diffusion of large molecular weight compounds into protein matrixes that act as model systems for the delivery of biomolecules and pharmaceutics. Thorough knowledge of both normal and anomalous diffusion in well-defined 3-dimensional structures is an integral part in the process of device creation and may also shed light on diffusion in cells.

We have described previously how three-dimensional micron scale protein matrixes can be readily cross-linked through the use of multiphoton excited (MPE) photochemistry.[5] This is because the desired photochemistry can be exclusively confined to the plane of focus through precise control of the laser power, just as in the more common technique of multiphoton excited fluorescence microscopy.[6] Multiphoton excited fabrication is a rapidly growing field, where most research has been directed at materials for 3-D data storage and photonic devices.[7−13]

Our primary interest lies in the area of developing the technology to create and characterize biomimetic and biocompatible devices for tissue engineering and controlled release applications. For example, we recently examined the kinetics of the enzyme alkaline phosphatase and, through Michaelis−Menten analysis, determined that bioactivity was maintained following cross-linking in protein and polymer matrixes.[14] In our earlier work,[5] we showed that the release rate of entrapped rhodamine dextrans from multiphoton photocrosslinked bovine serum albumin (BSA) matrixes was diffusion limited. However, this approach did not directly yield diffusion coefficients and also probed the release from the matrix rather than diffusion from within the interior and the release could have in fact been dominated by the two-dimensional properties of the surfaces. In this current work, we use the two-photon excited fluorescence recovery after photobleaching (FRAP) method within MPE cross-linked protein matrixes to directly measure the spatial dependence of the diffusion times of fluorescent dye model systems as a function of the fabrication conditions (controlled via the integrated laser flux, and thus mesh size) and tracer dye chemistry. Although conventional one-photon excited FRAP can be used to measure diffusion in three dimensions, this

* To whom correspondence should be addressed. Phone: 860-679-4354. Fax: 860-679-1039. E-mail: campagno@neuron.uchc.edu.

† Present address: Department of Chemistry, Bryn Mawr College, 101 N. Merion Ave., Bryn Mawr, PA 19010-2899.

10.1021/bm049707u CCC: $27.50
Published on Web 09/01/2004

is difficult because fluorescence is generated throughout the conical regions above and below the focal plane. By contrast, an accurate 3D map of diffusion can be directly obtained by the use of two-photon excitation for both the bleaching and monitoring process of the fluorescence recovery.[4]

We choose to fabricate BSA matrixes for this work as it is commonly used to create hydrophobic coatings in a wide range of biological applications. The fluorescent dyes (rhodamine B and Sulforhodamine variants and their respective dextran conjugates) have been selected based on their size, as well as their hydrophobicity, and hydrophilicity in order to exert both mass and chemical control over the diffusion properties. An important aspect of the current work is the direct observation of anomalous diffusion, and the ability to control its extent by varying the fabrication conditions.

Anomalous diffusion, i.e., where the diffusion coefficient is not constant, but rather time or spatially varying, is widely believed to be important in cell biology since this can have a major effect on the mobility of diffusing species (e.g., intracellular proteins) and, as a result, affect the kinetics of membrane and intracellular reactions. In vivo, this can arise from several factors including collisions with obstacles such as cytoskeletal proteins, spatially varying hydrodynamics, covalent and noncovalent interactions with cytoplasmic proteins.[15−17] Although anomalous diffusion has been studied both experimentally[17−20] and theoretically through Monte Carlo simulations,[21,22] it is still not well understood and is in fact difficult to isolate in live cells. Probing diffusion within 3D biomimetic structures created through multiphoton excited fabrication is an ideal method to study normal and anomalous diffusion since the composition and physical attributes can be totally controlled and studied systematically. The diffusion times are measured systematically for these chromophores as a function of integrated laser exposure (in effect the matrix mesh size), and we show the diffusion can be smoothly tuned in this manner. The trends in diffusion times are correlated both with the occupied protein volume fraction as determined by TEM, as well as by determination of the average mesh size using Flory-Rehner swelling analysis. These methods can then provide fundamental insight to guide the creation of microscale in vivo devices with a priori known properties over a wide range of diffusion by controlling the fabrication conditions.

Experimental Section

Materials. Bovine serum albumin (Calbiochem); Rose Bengal, Texas Red (Sulforhodamine 101), and rhodamine B, (Sigma, St Louis, MO); rhodamine-dextran (10 kD and 70 kD), Texas Red 10 kD dextran, and Texas Red-X methotrexate (Molecular Probes, Eugene OR), were used without further purification.

Fabrication Apparatus. The fabrication instrument is a home-built laser-scanning nonlinear optical microscope. As the design and performance have been previously described,[23] only the most important features are presented here. A femtosecond near-infrared titanium-sapphire oscillator (Mira 900-F, Coherent, Santa Clara, CA) is pumped by a 5 W Verdi Nd:YVO_4 (Coherent). The wavelength used for two-photon excitation of Rose Bengal for photocrosslinking as well as the FRAP experiments on the Texas Red and rhodamine chromophores was 806 nm. This wavelength is close to the two-photon absorption maximum for the latter dyes. The laser scanning is performed using a combination of two galvanoscanning mirrors (G120 and G138, GSI Lumonics, Billerica, MA) that are capable of line, raster, and outline scans of user-defined sizes. The software for both the scan control and simultaneous data acquisition was written entirely using LabVIEW 6.1 (National Instruments, Austin, TX), and a multi-purpose DAQ I/O board (National Instruments, PCI-6024E Austin, TX) is used to provide the drive signals to the Mini-Sax servo controllers for the scanning mirrors. The LabVIEW code is freely available on our website at http://www.cbit.uchc.edu/faculty_nv/campagnola/fabrication.html.

The two-photon excited fluorescence for the FRAP experiments is detected in an epi-illumination geometry using a nondescanned configuration. This approach provides greatly improved sensitivity, as a pinhole is not needed for nonlinear excitation. A R928 photomultiplier (Hamamatsu, Bridgewater, NJ) was used in single photon counting mode, and discriminated pulses were counted by the same 6024E DAQ multipurpose I/O board (National Instruments). TEM analysis was performed with Metamorph (Universal Imaging, Downingtown, PA) software.

Protein Cross-Linking and Fabrication Protocol. The two-photon excited photochemistry for Rose Bengal induced protein cross-linking has been described by us previously.[5,14] The xanthene photoactivator Rose Bengal is excited by two-photon excitation at 800 nm, which accesses the second excited state, S_2, which decays nonradiatively to S_1 and efficiently intersystem crosses to the reactive first triplet state. By examining the quenching effects of well-known free radical scavengers, the azide anion,[24] ascorbic acid, and 1,4-diazabicyclo[2,2,2]-octane (DABCO), we have shown that the protein cross-linking primarily proceeds through a singlet oxygen pathway.[14] This mechanism proceeds by reaction of singlet oxygen with an oxidizable amino acid residue of the protein. This irreversible mechanism generates an electron deficient protein that may react with another protein's amino acid residue to form a covalent bond. It has been shown by others that this scheme generally favors residues containing olefins, dienes, aromatics, and heterocycle groups including tryptophan, tyrosine, or histidine.[25,26]

Three-dimensional rectangular structures of proteins are created directly on a glass microscope slide by repetitive raster scanning until a visual change in the refractive index is observed, which is indicative of cross-linking or polymerization. Single layer structures were fabricated with dimensions 60 μm × 40 μm × 5 μm. Multilayered structures of BSA were fabricated by changing the focus of the microscope in 1 μm steps. The axial control of the microscope uses a stepper motor with a linear encoder (MAC 5000, Ludl Electronics, Hawthorne, NY) that is integrated in the LabVIEW code that drives the remainder of the experiment. Diffusion times are measured as a function of the integrated photon flux used during the fabrication. Furthermore, the

diffusion times are found to correlate with both TEM imaging and Flory-Rehner swelling analysis of the protein concentration and mesh, respectively.

Photobleaching Protocol and Analysis. Following fabrication, the protein structures were washed in water to remove any residual Rose Bengal that may have been entrapped in the matrix. For the photobleaching experiments, the fabricated samples were soaked in a 1 mM solution of the desired dye for 15 min to enable the dye to diffuse into the cross-linked protein matrix. The FRAP experiments were performed with a single-point bleach (nonscanning) near the center of the structure with laser pulse at full power (~100 mW at the sample), for approximately 5 s. The fluorescence recovery of the dye from the bleached region filling back in was monitored with repetitive line scans (every 100 ms) over a 15−100 second time course where the laser was attenuated by 70%. These measurements are repeated in 3−5 separated regions to obtain an average value and provide error bars. This FRAP method of point bleach/line scan probing has been used previously in order to obtain a spatial average in combination with a temporal response not possible with the point bleach/raster scan probe of the recovery.[27,28] Although in some of this work the structures are created and bleached in one layer, the recovery is in fact only probing interior regions of the structure. This is because the power densities used in the fabrication here result in an axial height (~5 microns) greater than the point spread function (PSF) of the 0.75 NA objective lens,[23] due to some saturation of the Rose Bengal chromophore. By contrast, the average power used for the monitoring results in an axial response of approximately 3 microns. It should be further noted that this exposure during the monitoring process is in fact much less per point than the 30% of the bleaching pulse as there are 300 pixels per line. In control experiments, we observe no significant bleaching during monitoring, thus no correction was made for this possibility. The resulting data were normalized, and at times near complete recovery, a five point running average was used to eliminate high-frequency noise. The temporal resolution of 100 ms arises from the computer interface to the scanning mirrors. This resolution is adequate for the current work since our time constants are on the order of several seconds.

MATLAB (The Mathworks, Natick, MA) was used to develop the routine to fit the fluorescence recovery data and extract the time constant, τ_D. Following Brown et al.,[4] we assume that the bleaching intensity distribution, I_{bl}, can be modeled using a 3D Gaussian approximation

$$\langle I_{bl}(r,z)\rangle = \langle I_{bl}(0,0)\rangle \exp\left[-\frac{r^2}{w_r^2}-\frac{z^2}{w_z^2}\right] \quad (1)$$

where w_r and w_z are the e^{-2} radial and axial dimensions. If the flow of dye back onto the BSA after bleaching follows diffusive behavior, the time dependent fluorescence signal, F, after photobleaching is[4]

$$F(t) = F_0\sum_0^\infty \frac{(-\beta)^n}{n!}\left(1+\left(1+\frac{2t}{\tau_D}\right)n\right)^{-1}\left(1+\left(1+\frac{2t}{R\tau_D}\right)n\right)^{-1/2} \quad (2)$$

where F_0 is equilibrium fluorescence signal, β is a bleach depth parameter, and $R = (w_z/w_r)^2$ is the square of the ratio of the $1/e^2$ beam dimensions.

For the case of anomalous diffusion, we follow the time dependent picture of Saxton[21] and we assume that the diffusion coefficient scales as, $D \propto t^{\alpha-1}$, which is equivalent to $\tau_D \propto t^{1-\alpha}$. Therefore, for anomalous diffusion, the fluorescence signal is

$$F(t) = F_0\sum_0^\infty \frac{(-\beta)^n}{n!}\left(1+\left(1+\frac{2t^\alpha}{\tau_D^\alpha}\right)n\right)^{-1}\left(1+\left(1+\frac{2t^\alpha}{R\tau_D^\alpha}\right)n\right)^{-1/2} \quad (3)$$

When $\alpha = 1$, the dye obeys normal diffusive behavior, whereas when α is less than 1, the diffusion is anomalous. Fits to the data were done using the Marquardt method[29] on eq 3 solving for the parameters F_0, β, τ_d, and α. Our purpose is primarily to compare diffusion times in cross-linked protein matrixes and not to report absolute diffusion coefficients. However, to simply provide an order of magnitude, the lateral diffusion coefficient, D, is related to the diffusion time by the following equation (for two-photon excitation):[4]

$$D = \frac{w_r^2}{8\tau_D} \quad (4)$$

The $1/e^2$ height for the 0.75 NA objective lens was calculated to be 1.3 μm based on the point spread function (PSF) data we previously reported for our microscope[23] as well as by SEM data presented in the next section.

Results and Discussion

3-D Matrix Characterization. Due to the optical sectioning, multiphoton excited polymerization is, in principle, a freeform 3D fabrication method. Thus, nanoscale and microscale objects can be created with attributes such as overhanging features and channel structures that would be virtually impossible to create by the more common fabrication methods of photolithography and microcontact printing. We have previously shown examples of stacked and channel structures created from hydrogels (polyacrylamide) and protein structures in aqueous environments.[5,30] Figure 1a shows the SEM image of 2 stepped pyramid structures, where the 3 levels were created by changing the focus and zooming in to create subsequent smaller layers. In the following work, we will use 3D rectangles consisting of both single layer and multiple layered structures to measure the diffusion, although more complex structures could have also been employed. Scanning transmitted light is a useful diagnostic on the micron scale to probe the uniformity of polymerized or cross-linked structures, as these processes result in a change in the index of refraction. Figure 1b shows the corresponding image for a typical cross-linked BSA structure used for the diffusion measurements. The fabrication is seen to be fairly uniform, except at the edges, which arises from flyback of the galvo scanner.

Resolution of MPE Fabrication of Protein Structures. We previously determined the optical performance of the

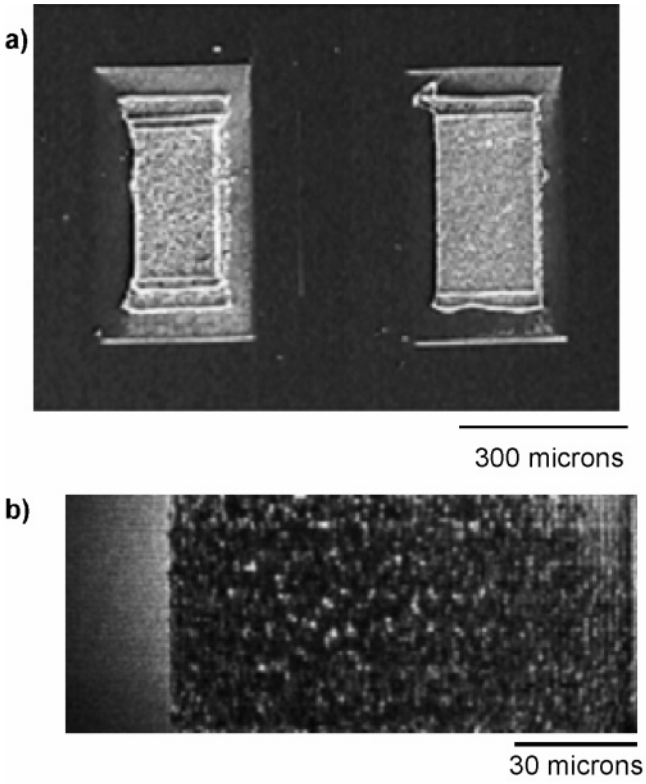

Figure 1. Images of 3D BSA structures fabricated by multiphoton excited photochemistry: (a) SEM image of two stepped pyramid structures, where the three levels were created by changing the focus and zooming in to create subsequent smaller layers. Reprinted with permission from Pitts et al. 2000. (b) Scanning transmitted light of the BSA matrixes used for the diffusion measurements.

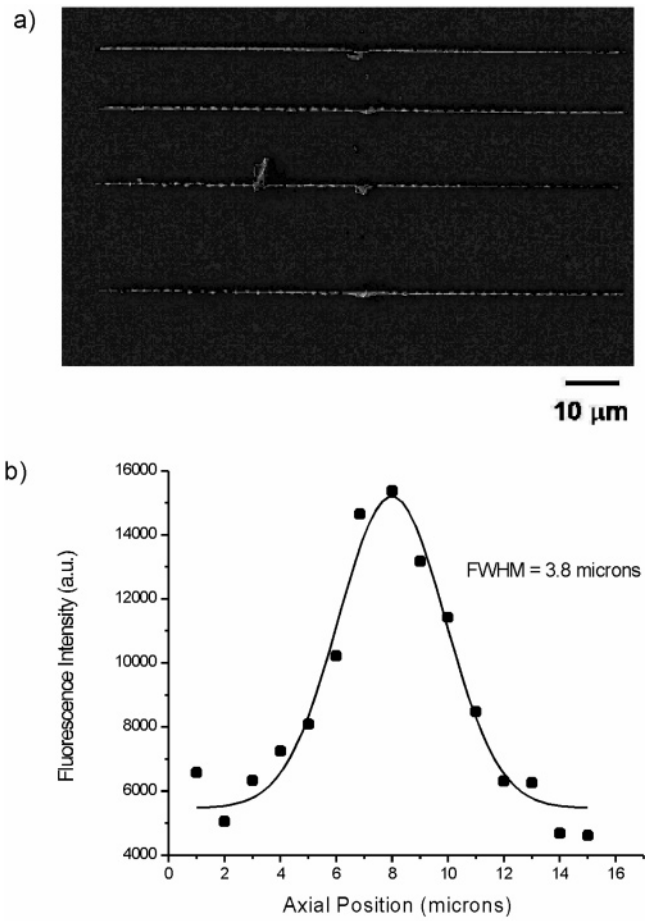

Figure 2. Resolution of multiphoton excited fabrication with the protein BSA. (a) lateral resolution is determined by SEM measurements to yield widths of 600−700 nm; (b) axial resolution of rectangular matrixes is determined by measuring the height at higher NA, and the resulting fit has fwhm of 3.8 microns.

laser scanning microscope at high numerical aperture by measuring the axial and lateral point spread functions by imaging the fluorescence of sub-resolution 100 nm labeled beads[23] and achieved good agreement with results from other workers,[31,32] where we determined a lateral PSF of 430 nm at 1.3 NA. Since the determination of the diffusion coefficient, *D*, in eq 4 is dependent on the lateral PSF, and the axial response is important in creating multilayer structures, we determine the "resolution" limits for fabrication of the protein structures (NA = 0.75) used for the diffusion measurements to follow in the next section. The most convenient object to determine the lateral limit of fabrication is a rod, which is created by repetitive line scanning. Figure 2a shows the resulting SEM of 4 rods of BSA fabricated using a 0.75 NA lens, where the widths of these rods are between 600 and 700 nm. Comparable values have also been obtained by higher resolution fluorescence imaging (1.3 NA) of residual Rose Bengal in the structure. Most theoretical predictions of resolution[33,34] are based on fluorescence methods; however, as an approximation, we can extrapolate the measured 1.3 NA PSF to provide an estimate of the predicted width of these lines. Using the ratio of the numerical apertures [1.3/0.75] and using the measured 430 nm lateral PSF, a fabricated width of 745 nm would be predicted. Thus, the fabrication lateral "resolution" measured both by SEM and fluorescence is in good agreement with the predicted optical resolution. To obtain an estimate of the axial resolution in fabrication of protein structures, we constructed a one level BSA matrix at 0.75 NA, and then we measured the step height using a 1.3 NA objective. This resulted in a minimum height of ~3.5 microns for this lens. Given the axial PSF of 900 nm measured above for 1.3 NA excitation, and then scaling the axial resolution by the ratio of NA,[2] the predicted value for 0.75 NA would be 2.7 microns. Thus, the measured value is in reasonable agreement with that predicted by theory. More importantly, in most of the diffusion measurements to follow, the matrixes have heights of 6−15 microns, thus interior regions can be probed without significant surface contributions.

Matrix Mesh Sizes and Protein Concentration. To fully characterize the diffusion within microfabricated protein structures, we need to characterize the mesh sizes, the fractional protein coverage, and actual concentration in the matrixes as a function of the laser exposure. Here we define the laser exposure in terms of integrated photons per pixel and since the fabrication is performed at the same wavelength and same pulse width, this measurement provides internally consistent results, as previously described.[30] We first use a variation of the Flory-Rehner method to accurately calculate the average mesh size of the BSA structures used in this work. The underlying physics is that tighter cross-linked structures will swell (or shrink) less than less tightly cross-linked structures. Leach and co-workers used a similar approach to calculate the relative degree of cross-linking in glycidyl methacrylate-hyaluronic acid (GMHA) hydrogels.[35]

Table 1

laser dose (μJ)	height (dry) (μm)	height (wet) (μm)	$Q_v^{1/3}$	$\xi = Q_v^{1/3}\sqrt{r_0^2}$ (nm)
7	3.72	6.5	1.75	390 ± 53
10	3.95	5.8	1.47	328 ± 47
15	4.89	5.9	1.21	270 ± 38
20	4.94	6.5	1.32	294 ± 42
25	4.05	5.2	1.28	285 ± 40

This method relates the volumetric swelling ratio, Q_v, to the hydrogel mesh size, ξ, according to the following equation:

$$\xi = Q\upsilon^{1/3}\sqrt{r_0^2} \tag{5}$$

where r_0^2 is the root-mean square distance between the cross-links and for BSA, this distance is the hydrodynamic diameter as measured by Bowen and co-workers.[36] The root-mean square distance is related to this diameter as follows:

$$\left(\frac{r_0^2}{2n}\right)^{1/2} \cong 6.4 \text{ nm} \tag{6}$$

where n is the number of repeat units or residues in the protein, and $n = 607$ for BSA. The swelling experiments were carried out as follows. First, BSA structures were fabricated over a four- fold range of laser exposure (5−20 μJ). After the structures were soaked in water, the heights of the "wet" or "swollen" structures were then measured at 1.3 NA by using fluorescence of the entrapped Rose Bengal. The heights of the "dry" structures were measured after dehydrating the proteins with repeated methanol washes, followed by air-drying for 15 min. Re-hydration reproduced the initial wet heights. Since swelling is taking place in three dimensions, the swelling ratio, $Q_v^{1/3}$ is simply taken as the ratio of the step heights. The data are summarized in Table 1. It is seen that with increasing laser exposure, the calculated mesh size decreases by approximately 30% and then reaches an asymptotic limit. A similar asymptotic limit is observed in the measured diffusion times, τ_d, and, as we will show, this corresponds to the terminal cross-linking limit of using all available reactive residues. These mesh sizes are in the range of a few hundred nm and are in agreement with our previous qualitative observations by lower resolution SEM imaging. We will show in the next section that, depending on the tracer dye chemistry, this decrease in mesh sizes translates into a decrease of approximately 5 to 10-fold in diffusion.

We measured analogous swelling data for two different initial concentrations of BSA (4.5 and 9 mg/mL) as a function of laser exposure to determine if the protein concentration and mesh sizes can be independently controlled. Indeed, different swelling ratios were found for the two cases, where the lower concentration swelled more significantly. Assuming the cross-linked protein concentration is proportional to the initial concentration in solution, this suggests that, at least over a certain range, that the protein concentration and mesh sizes can be tuned independently.

We next use TEM imaging to examine the protein assemblies at magnification beyond the optical limit. Protein matrixes were first fixed in gluteraldehyde,[5] encapsulated in polymer, stained with uranyl acetate, sectioned and then imaged at 15.5 K magnification. Representative images at low, intermediate, and high laser exposure are shown in Figure 3, parts a−c, respectively. Although a range of mesh sizes clearly exists, the fractional area of the protein (dark contrast) increases at higher laser exposure. A spread of mesh sizes was also observed in previous SEM images of cross-

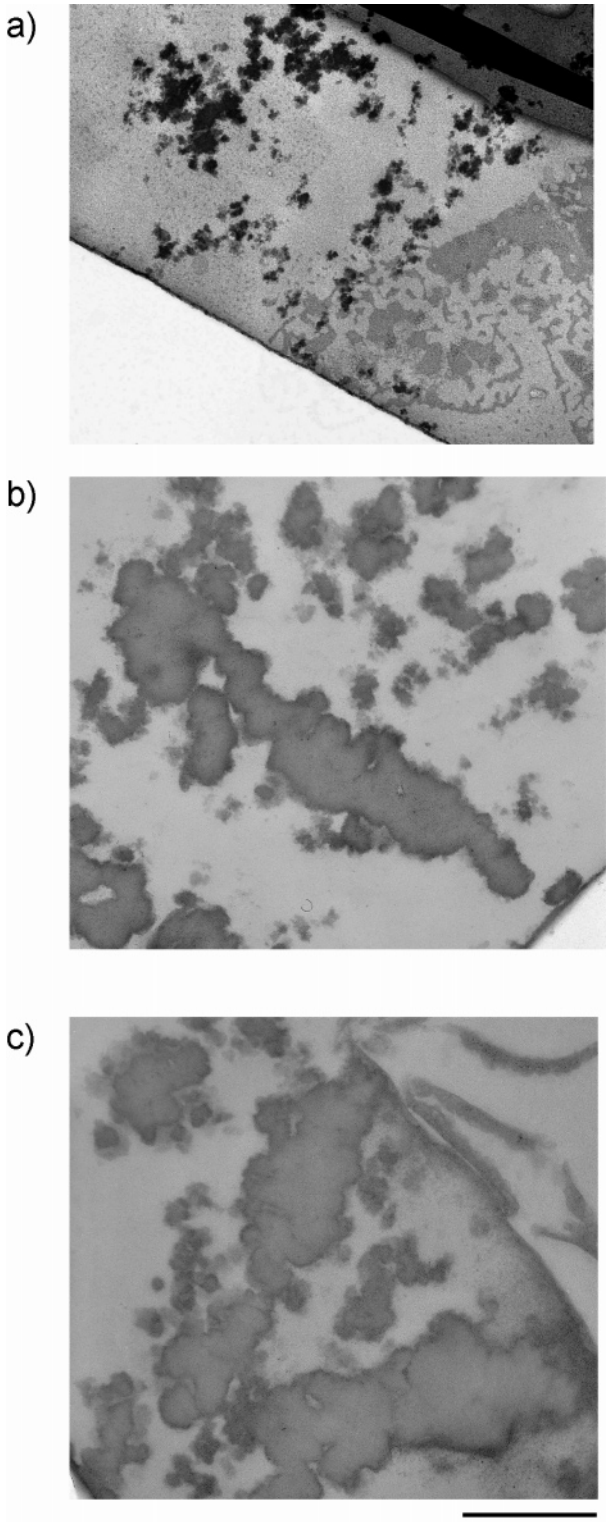

Figure 3. TEM images of BSA matrixes fabricated with increasing laser exposure of (a) 5, (b) 12, and (c) 20 μJ. The protein stained areas in (a) correspond to the very dark portions. The fraction of protein increases from 13% in (a), 46% and 62% in (b), and (c), respectively. Scale bar = 1 micron.

linked BSA matrixes.[5] Determination of the protein coverage areas was achieved using Metamorph software to threshold the images, followed by integration of the protein areas, and then averaged over several fields of view. The resulting fractional areas for low, intermediate, and high laser exposure are 13% (±2), 46% (±3), and 62% (±12), respectively, and as described above, these correspond to a sharp decrease in the measured diffusion.

Below the limit of terminal cross-linking (to be shown below), the diffusion times will result from a combination of both the protein cross-linking density and the actual protein concentration in the matrix.[14] To determine the actual protein concentration, we take a ratiometric approach by cross-linking fluorescently labeled BSA (Texas Red) and comparing the fluorescence in the starting solution to that in the cross-linked protein matrix. Several BSA matrixes were fabricated over a large range of laser exposure and the fluorescence of the Texas Red-BSA conjugate was then measured using two-photon excitation at 830 nm. Since there is no appreciable Rose Bengal two-photon absorption at this wavelength and the Texas Red fluorescence quantum yield is much greater than that of Rose Bengal (at least 50-fold), the measurement is essentially background free. In solution, we observe no fluorescence quenching at this concentration range. The fluorescence of the cross-linked protein at the highest laser exposure (and terminal cross-link density) was approximately 8 times that in free solution and about 5-fold larger for lowest exposure (5μJ).

Spatial Control of Diffusion within Cross-Linked Protein Matrixes. A main goal in assessing this technology for biomaterials applications is to examine the 3-D spatial control possible with the fabrication method. To this end, we fabricated BSA matrixes consisting of 10 overlapping layers and measured the diffusion throughout the axial range of the structure. Each layer was spaced by one micron, and since the axial PSF of the objective used for fabrication is approximately 3 microns, there is considerable overlap between the layers, and the overall height is about 15 microns. It should be noted that, although we are using the MPE fabrication process to create rectangular structures for simplicity, it would be difficult to create comparable multilevel matrixes by other methods such as masking or microcontact printing without altering preexisting layers. Then we exploit the three-dimensionality offered by two-photon excitation to FRAP measurements, to obtain a three-dimensional map of the diffusion. A sample recovery curve from one such layer for Texas Red in BSA is shown in Figure 4a, along with the fit from eq 2, that yields a τ_D of 3.5 s. We repeated this measurement throughout the axial range of the structure starting at the interface between the glass slide and the first layer and ending near the top. Figure 4b shows the spatial dependence of the diffusion of Texas Red at various levels of such multilayered BSA structures fabricated in two different ways. For convenience, we plot the data in terms of $1/\tau_D$, as this is proportional to the diffusion coefficient. The first, with the data denoted by squares, was constructed by equal laser exposure at all axial layers. This structure displays the fastest diffusion at the interface between the glass surface and the protein structure,

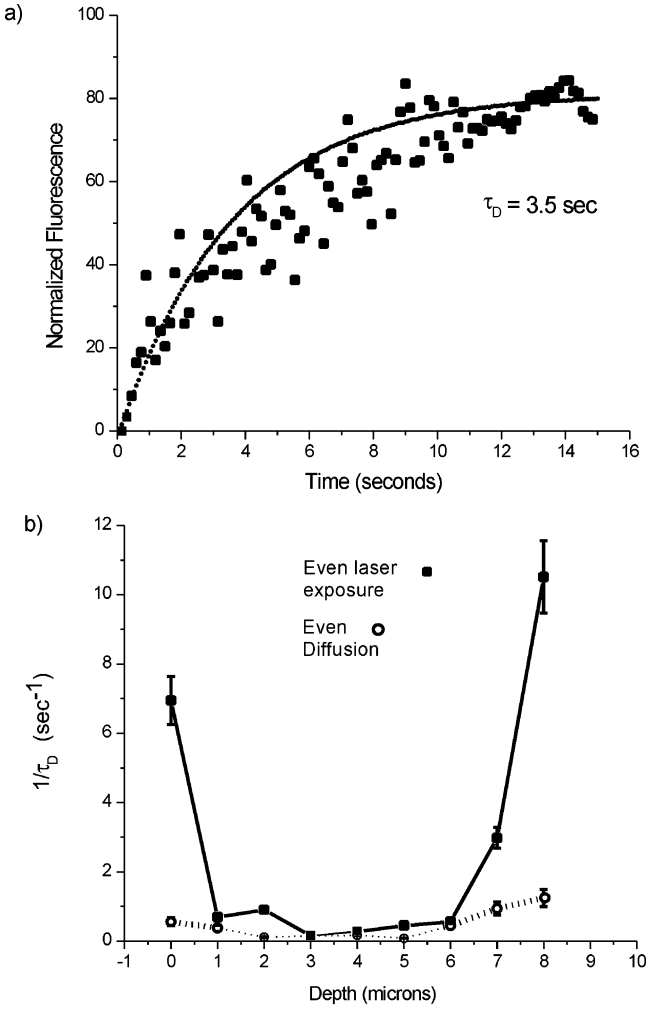

Figure 4. (a) Typical fluorescence recovery plot for Texas Red (sulforhodamine 101), along with the corresponding fit from eq 2, resulting in a τ_D of 3.5 s. (b) Axial dependence of the diffusion for Texas Red through a 10 layer, 15 micron thick BSA matrix. The data are plotted as the inverse of the diffusion time ($1/\tau_D$) to be proportional to the diffusion coefficient. The squares correspond to a structure that was created with equal laser exposure at all levels, and faster diffusion is observed at the top and bottom due to lack of overlap in the individual layers. Uniform diffusion (circles) is observed for the structure created with higher exposure at the extrema to match the overlap in the interior.

and arises from the combined effects of enhanced diffusion near walls and edges and the fact that the bottom layer is less tightly cross-linked than the interior layers that are heavily overlapped. Similar diffusion times are measured in the middle layers and imply comparable average mesh size and protein concentration throughout this region. It should be noted that sampling different lateral regions at the same axial position yields similar values of τ_D. Similar to the bottom layer, the diffusion shows a gradual increase toward the top of the structure. Overall, an almost 20-fold range in diffusion was obtained while simply maintaining constant laser flux. This same depth-dependent behavior was recently reported by Van Keuren and Schrof[37] where they measured the diffusion of rhodamine B in thin polymer films (poly(vinyl alcohol)) created through regular chemical polymerization.

Since our fabrication method has three-dimensional spatial control, it should be possible, by varying the laser exposure

at the top and bottom layers, where there is less overlap of layers, to achieve nearly uniform diffusion throughout the axial range of the structure. This was indeed accomplished by exposing these regions to more integrated photon flux (3-fold) and then gradually decreasing the dose until the middle layers' interior portions were fabricated. The results are shown in Figure 4b (data denoted by the circles), and it is observed that within the error of the experiment nearly uniform diffusion is obtained throughout the structure. The effect of the enhanced diffusion at the surfaces can be thus compensated by increasing the extent of cross-linking in these regions. The ability to control the diffusion in all three dimensions gives credence to using this fabrication technology to eventually use such microfabricated structures as real devices.

Effect of Dextran Molecular Size on Diffusion Time. In this work, we use both low and high molecular weight dyes as models for drugs and bioactive molecules such as growth factors. It is important then to establish if diffusion-limited responses within cross-linked protein matrixes are obtained for these two different size regimes. To this end, we compare the diffusion times for 10 and 70 kD rhodamine B dextrans within BSA matrixes. For self-consistency, the BSA matrixes in each case were created under identical optical conditions, i.e., the same integrated photon flux (20 μJ) and the same size structure. The fluorescence recovery data for the two rhodamine dextrans are shown in Figure 5a along with the corresponding fit to eq 2. The 10 and 70 kD data were fit with τ_D values of 0.81 and 1.63 s, respectively. In the simplest picture of diffusing molecules as uniform spheres, the diffusion should scale as the cube root of the mass. Thus, the 10 and 70 kD moieties should have scaled by 1.9, whereas a ratio of 2.5 was obtained. Although this is not in perfect agreement, dextrans are best described as random coils, and the ratio of the radii has been recently measured as 2.5[38] and in good agreement with our diffusion data.

We will show below that both the rhodamine B and the 10 kD dextran are well-characterized by normal diffusion, whereas reliable values for the anomalous diffusion coefficient for the 70 kD moiety were not obtainable. This is also corroborated by examination of the fractional recoveries of the rhodamine B, and the two dextrans. At terminal cross-link density (to be shown below), rhodamine B and the 10 kD dextran displayed fractional recoveries of approximately 80−90%. These values are indeed typical for nearly freely diffusing species.[4,39] By contrast, at similar porosity, the fractional recovery for the 70 kD dextran was approximately 50%, indicating that the diffusion was substantially hindered for the larger species. Popov and co-workers[40] also observed similar deviations in scaling from simple size considerations diffusion of dextrans which they attributed to hindrance from interactions of the larger dextran with cytoplasmic components.

Effect of Fabrication Conditions on Diffusion. A fundamental issue concerning the use of microfabricated structures as delivery devices is whether diffusion-limited behavior is obtained and over what range of chemical properties of the matrix and diffusing species this condition holds. Thus, the next step is to measure the diffusion of

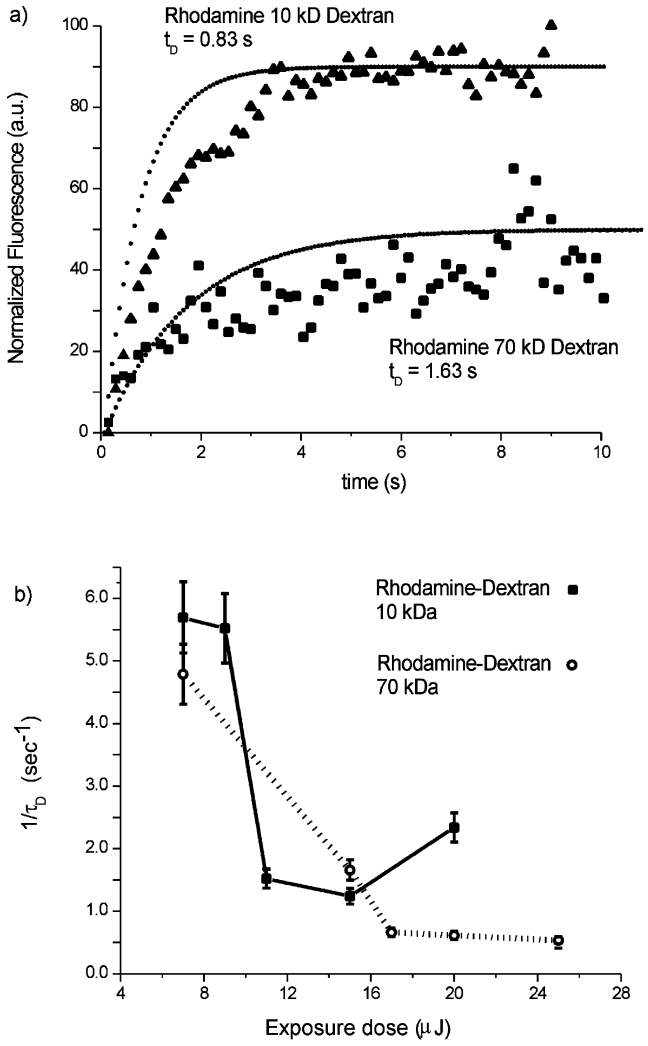

Figure 5. Comparison of the diffusion of rhodamine 10 and 70 kD dextrans in BSA: (a) Sample fluorescence recovery data for the two dextrans at the same laser exposure with corresponding τ_D values of 0.83 and 1.63 s, respectively. (b) The dependence of the diffusion ($1/\tau_D$) as a function of the laser exposure. For both molecules, a smooth asymptotic decrease in diffusion is observed as the mesh size decreases and protein concentration increases. The asymptote corresponds to the terminal cross-link density, when all available reactive surface sites are used.

rhodamine and its dextran conjugates as a function of the mesh size and concentration of the BSA host matrix. The correlation of these properties with laser exposure was shown earlier in the TEM data in Figure 3 and the mesh size determinations in Table 1. The resulting τ_D values are tabulated in Table 2. For consistency with the convention in Figure 4, we then plot the inverse diffusion times as a function of the integrated laser exposure, and the results are shown in Figure 5b. The plot shows a nearly smooth decline in diffusion as a function of exposure dose for the two rhodamine dextrans. The diffusion of rhodamine B (not shown), whose molecular weight is significantly lower than the rhodamine−dextrans, could not be measured at the lower exposure doses as the diffusion was occurring on a faster time-scale than our experiment could measure. All of the dyes exhibit a sharp decrease in the diffusion at increasing exposure dose until the asymptotic limit of cross-link density is reached. We determined this limit by sequential additional of photoactivator, protein, and additional laser flux, and we

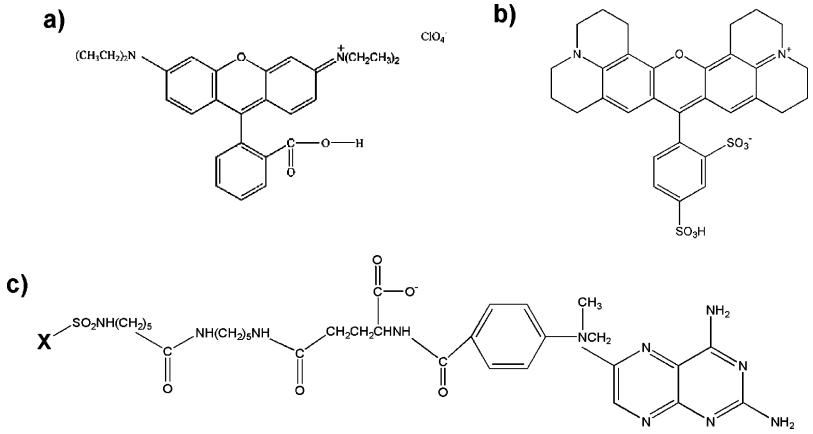

Figure 6. Chemical structures of the chromophores used in this work. (a) Rhodamine B, MW = 479 amu, (b) Texas Red, or sulforhodamine 101, MW = 606 amu, and (c) Texas Red methotrexate, MW = 1257 amu.

Table 2

	diffusion times, τ_D (s)					
laser dose (μJ)	rhodamine B, FW = 479	Texas Red, FW = 606	Texas Red−NH_4, FW = 1257	Texas Red−dextran, 10 kDa	rhodamine−dextran, 10 kDa	rhodamine−dextran, 70kDa
6		0.19 ± 0.02	1.68 ± 0.17			
7			1.85 ± 0.18	0.18 ± 0.02	0.18 ± 0.02	0.21 ± 0.02
9					0.18 ± 0.02	
10		0.21 ± 0.02				
11			1.56 ± 0.16	0.33 ± 0.03	0.66 ± 0.07	
15	0.22 ± 0.02		2.06 ±0.20	2.26 ± 0.23		0.60 ± 0.06
17		4.33 ± 0.43	6.55 ± 0.65			1.51 ± 0.15
20	0.79 ± 0.08			4.89 ± 0.49	0.81 ± 0.08	1.63 ± 0.16
25	1.81 ± 0.18	3.12 ± 0.30	6.12 ± 0.60		0.43 ± 0.04	1.87 ± 0.19

observed no increase in the diffusion times,[14] which would have corresponded to slower diffusion. Gilbert,[41] who in nonphotochemical synthesis (centimeter scale) also observed a decrease in diffusion coefficients with increased cross-link density, concluded that this inverse relationship is due to a decrease in porosity in the protein matrix. Similar behavior was also noted by Ushiki[42] for the diffusion of rhodamine B in polyacrylamide gels. Although our work is on the microscale, it is seen that through the use of laser scanning multiphoton excited cross-linking the diffusion within protein matrixes can be controlled in a smooth and reproducible manner.

Anomalous Diffusion of Texas Red Dyes. In the previous section, we demonstrated how the diffusion can be spatially controlled through changing the laser exposure and thus mesh size of the BSA matrix. Now we show that the chemistry of the diffusing species can be also chosen to control the diffusional properties. In particular, we show that by replacing the hydrophilic rhodamine B chromophores with hydrophobic sulforhodamine Texas Red dyes results in well-controlled but highly anomalous diffusion. The structures of rhodamine B and two Texas Red derivatives, sulforhodamine 101 and the Texas Red X-methotrexate, are drawn in Figure 6.

One simple manifestation of anomalous diffusion is a significant deviation from scaling with molecular weight, such as a lighter species diffusing much slower than heavier molecules. As discussed earlier, there are various physical mechanisms that give rise to anomalous diffusion including binding (covalent and noncovalent) and collisional interactions. Here we investigate the role of potential traps formed by the attraction of the hydrophobic Texas Red dyes and the hydrophobic surface of the BSA molecules in the cross-linked matrix. The molecular weights of rhodamine B and Texas Red are 479 and 606 amu, respectively, and thus, from simple mass considerations, would be expected to have comparable diffusion times. Further, it would be expected that the diffusion of Texas Red would be considerably slower than that of the higher molecular weight rhodamine dextrans. The resulting inverse diffusion times of Texas Red, Texas Red methotrexate, and 10 kD Texas Red dextran are plotted in Figure 7 as a function of laser exposure and also are summarized in Table 2. Although these three Texas Red dyes qualitatively display the same smooth, asymptotic decrease in the diffusion with increasing laser dose as the rhodamines, from a quantitative perspective the results are in fact very different. For example, at the same integrated laser exposure, the diffusion for Texas Red methotrexate (amu = 1257) was 10-fold smaller than rhodamine B (not shown). Second, and perhaps more surprising, the diffusion for the Texas Red 10 kD dextran is in fact comparable or *much higher* than the lower molecular weight unlinked moieties (606 and 1257 amu, respectively). Third, the diffusion for the higher molecular weight methotrexate moiety is a few-fold slower than the regular Texas Red and is thus considerably slower than predicted by simple size considerations. Based on mass, the diffusion for the two lower molecular weight Texas Red is clearly anomalous, when compared to the hydrophilic rhodamine or the Texas Red 10 kD dextran. This most likely arises from the favorable hydrophobic binding interactions

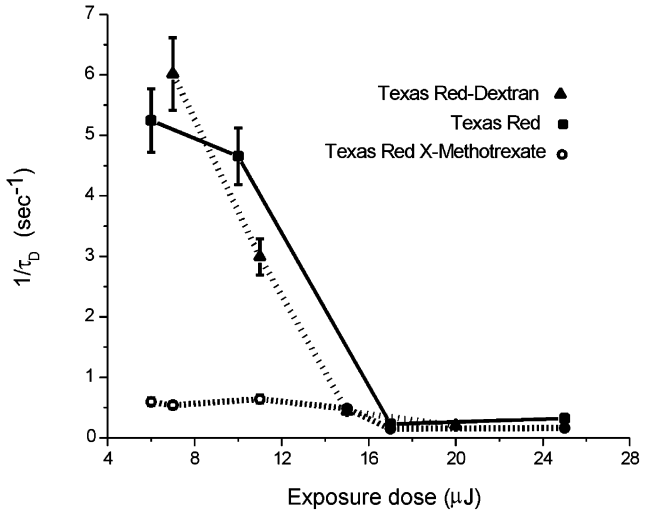

Figure 7. Comparison of the diffusion ($1/\tau_D$) of Texas Red, Texas Red methotrexate, and Texas Red 10 kD dextran in BSA as a function of integrated laser exposure. Similar to the rhodamines in Figure 5, for all three molecules, a smooth asymptotic decrease in diffusion is observed as the laser dose increases (and mesh size decreases). The diffusion is more rapid for the 10 kD dextran than that of the unlinked Texas Red moieties, indicating the diffusion is highly anomalous.

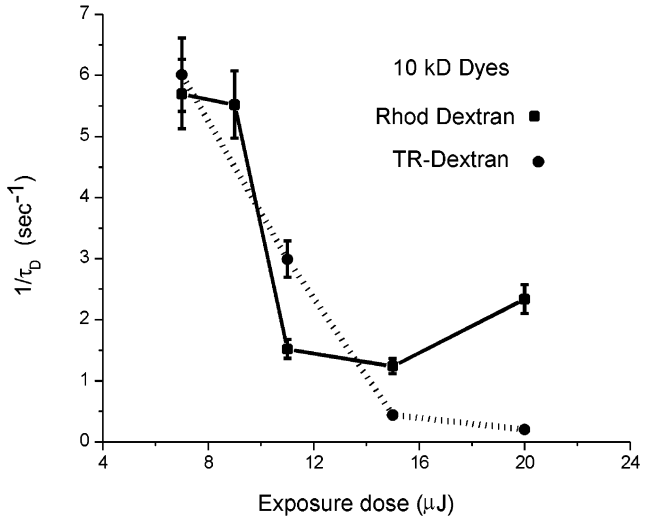

Figure 8. Comparison of the diffusion ($1/\tau_D$) of rhodamine and Texas Red 10 kD dextrans as a function of integrated exposure dose. For most of the range, the diffusion is comparable, indicating it is dominated mainly by the hydrophilic dextran, rather than the hydrophobicity or hydrophilicity of the chromophores.

between the dye and the BSA. Through Monte Carlo simulations, Saxton predicted similar results, suggests that binding will only produce anomalous diffusion if the binding residence time is "undefined"; that is, the length of time that a molecule remains bound decays like a power law of the time rather than as an exponential. If binding, rather than obstruction, is leading to the anomalous diffusion we report here, it suggests that the binding residence time is variable; that is, it is not exponentially distributed.

To examine this further, the inverse diffusion times for the respective Texas Red and rhodamine B 10 kD dextrans are plotted as a function of the laser dose in Figure 8. It is seen that these two 10 kD moieties have quite similar diffusion at low dose. This probably arises from that fact that the dextrans are hydrophilic and the hydrophobic chromophore of the Texas Red dextran comprises only a small portion of the mass and surface. Thus, it is reasonable that these two dextrans would have similar diffusion times even with the difference in hydrophilicity of the chromophore. At terminal cross-linking, the diffusion of the rhodamine B dextran decreases less than the Texas Red dextran, which may result from the effect that as the mesh of the BSA matrix becomes smaller, the diffusion is more hindered, and the interaction of the smaller hydrophobic chromophore with the BSA becomes more important. The extent that the diffusion is anomalous can be determined more quantitatively by fitting the fluorescence recovery data to eq 3, which includes the anomalous diffusion coefficient α, where the normal and anomalous cases are defined as $\alpha = 1$ and $\alpha < 1$, respectively. We only accept values of α when the fits to eqs 2 and 3 yield the same value of τ_D. The resulting values for α at two ranges of exposure are given in Table 3. In the first row (exposure dose 12 μJ), it is seen that the rhodamines have values very close to unity and are thus described in the normal regime. Similarly, the 10 kD Texas Red dextran with $\alpha = 0.9$ also is in the normal regime and is consistent with the similarity of the two different dextrans shown in Figure 8. By contrast, Texas Red and the methotrexate derivative are highly anomalous with values of 0.3 and 0.8, respectively.

The results for diffusion within highly cross-linked matrixes (shown in the second row of Table 3) are in fact quite different. At near terminal cross-linking densities (20 μJ), these values for α for the Texas Red is approximately 0.8 indicating that while the diffusion is still, anomalous, it is to a lesser extent. The diffusion of the methotrexate remained highly anomalous, which may be consistent with its translation being greatly hindered, as suggested by the data in Figure 7. By contrast, rhodamine B, its dextran conjugates, as well as the Texas Red dextran displayed near unity α values and thus normal diffusion at all values of laser exposure. These trends may be explained in terms of effective concentrations of binding species or obstacles and the tracer dyes.

Previous theoretical[21,22] and experimental studies[37] have examined anomalous diffusion by measuring the concentration dependence as a function of the concentration of obstacles or binding sites. We have taken the inverse tact of keeping the concentration of the protein constant and varying the tracer concentration and measured the recovery times at constant exposure dose ($\sim$12 μJ) as a function of concentration for the normally diffusing rhodamine B 10 kD dextran

Table 3

dye	rhodamine B	rhodamine B, 10kD	Texas Red	Texas Red, 10 kD	Texas Red−NH_4
α low dose	1.0	0.95−1.0	0.3	0.9	0.8
α high dose	0.8	0.85	0.8	1.0	0.6

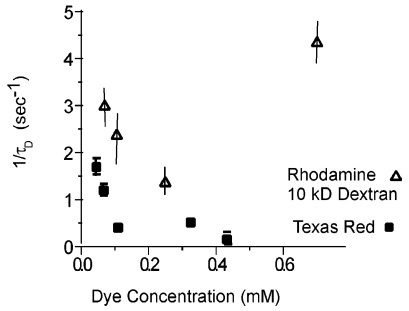

Figure 9. Comparison of the concentration dependence ($1/\tau_D$) of the diffusion for rhodamine 10 kD dextran and Texas Red (sulforhodamine 101) in BSA matrixes constructed at identical integrated laser exposure. The former shows no dependence on concentration, and is consistent with the characterization of the diffusion as being normal from near unity values of α in Table 3. By contrast, Texas Red shows a strong decrease in diffusion at higher concentrations, presumably due to increasingly probable interactions with the hydrophobic protein, and is consistent with the subunity values of α in Table 3.

($\alpha \sim 1$) and the somewhat anomalous Texas Red in the region where $\alpha \sim 0.8$. The data are shown together in Figure 9. There is no discernible concentration dependence on the recovery time for the rhodamine B dextran in the BSA matrix. A similar trend was also observed for the 10 kD Texas Red dextran (data not shown). This is consistent with the lack of strong affinity between the hydrophilic dye and the hydrophobic protein. However, there is a marked concentration effect for the Texas Red, where at higher concentrations, the diffusion becomes increasingly anomalous. This is because there is a statistically higher probability of noncovalent binding between the dye and the protein host at high concentrations. In our experiment, the concentration of cross-linked BSA is approximately 1.5 mM and is higher than the dye concentration even at the highest point of ~0.5 mM. It is possible that at very high concentrations a lower fraction of the dye (yet higher absolute numbers) can bind, and self-association will become important. Given that the τ_D's of the rhodamine dextran as well as Texas Red dextran (data not shown) have no concentration dependence, we do not believe we are yet in this regime, as they would be expected to have to same behavior as the hydrophobic Texas Red. The average pore sizes, as determined by the swelling experiments, are in the range of several hundred nanometers, and the association of dye molecules, either bleached or unbleached, would not have a significant effect on the resulting pore size. In sum, these examples point out that both normal and anomalous diffusion within structures created by the multiphoton excited fabrication can be well-controlled simply by altering functional groups on the diffusing species.

To understand the chemical origins of this highly anomalous behavior in the Texas Red dyes, we examine differences in the structures of rhodamine B and Texas Red that give rise to the hydrophobicity of the latter. Compared to rhodamine B (Figure 6a), Texas Red (Figure 6b) is likely to be more hydrophobic due to the ring structure that restrains the nitrogen atom. In rhodamine B, the nitrogen atoms are attached to alkyl chains and are not constrained by the aromatic ring. A restrained nitrogen atom will have its lone pair exposed and be able to interact with amino acid residues in BSA. Texas Red X-Methotrexate (Figure 6c) has several additional restrained nitrogens and its diffusion is yet more hindered than Texas Red 101, and significantly slower than predicted by mass scaling (see Table 2). This may also arise, in part, from mechanical considerations from the long chain extending from the aromatic ring structure. Structural aspects of the protein may also be important in determining if the diffusion is characterized as normal or anomalous. For example, Somorjai[43] has shown that the packing of fibrinogen, BSA, and lysozyme was strongly dependent upon the hydrophilic or hydrophobic nature of the surface.

Conclusions

We have demonstrated that the diffusion properties within three-dimensional cross-linked protein matrixes constructed through multiphoton excited photochemistries can be tuned through both spatial and chemical control. By altering the fabrication conditions, a wide range of diffusion times can be obtained throughout a multilayer 3D matrix. We also observe that the mesh size and protein concentration of the matrix have a profound effect on the diffusion. The diffusion of the hydrophobic and hydrophilic tracer molecules can be greatly affected by noncovalent interactions within the protein host, leading to highly anomalous diffusion. Thus, 3D matrixes cross-linked by MPE photochemistires may be a good model system to systematically study the molecular effects that give rise to anomalous diffusion. These results suggests the possibility of chemical modification of a desired species such as a drug to greatly alter its mobility in a microscale environment that can be fabricated with a priori knowledge of it properties.

Acknowledgment. Support under NIH R01 EB000263 is gratefully appreciated. We also thank Dr. Mark Zajac and Dr. Andrew Millard for technical assistance, Dr. John Aghajanian for assistance with the TEM experiments, and Dr. Leslie Loew and Dr. Ann Cowan for helpful discussions.

References and Notes

(1) Arrio-Dupont, M.; Foucault, G.; Vacher, M.; Devaux, P. F.; Cribier, S. *Biophys. J.* **2000**, *78*, 901−907.
(2) Gribbon, P.; Hardingham, T. E. *Biophys. J.* **1998**, *75*, 1032−1039.
(3) Braeckmans, K.; Peeters, L.; Sanders, N. N.; De Smedt, S. C.; Demeester, J. *Biophys. J.* **2003**, *85*, 2240−2252.
(4) Brown, E. B.; Wu, E. S.; Zipfel, W.; Webb, W. W. *Biophys. J.* **1999**, *77*, 2837−2849.
(5) Pitts, J. D.; Campagnola, P. J.; Epling, G. A.; Goodman, S. L. *Macromolecules* **2000**, *33*, 1514−1523.
(6) Denk, W.; Strickler, J. H.; Webb, W. W. *Science* **1990**, *248*, 73−76.
(7) Strickler, J. H.; Webb, W. W. *Opt. Lett.* **1991**, *16*, 1780−1782.
(8) Albota, M.; BeLjonne, D.; Bredas, J.-L.; Ehrlich, J. E.; Fu, J.-Y.; Heikal, A. A.; Hess, S. E.; Kogej, T.; Levin, M. D.; Marder, S. R.; McCord-Maughon, D.; Perry, J. W.; Rockel, H.; Rumi, M.; Subramaniam, G.; Webb, W. W.; Wu, X. L.; Xu, C. *Science* **1998**, *281*, 1653−1656.
(9) Zhou, W.; Kuebler, S. M.; Carrig, D.; Perry, J. W.; Marder, S. R. *J. Am. Chem. Soc.* **2002**, *124*, 1897−1901.
(10) Witzgall, G.; Vrijen, R.; Yablonovitch, E.; Doan, V.; Schwartz, B. J. *Optics Lett.* **1998**, *23*, 1745−1747.
(11) Kawata, Y.; Ishitobi; Kawata, S. *Opt. Lett.* **1998**, *23*, 756−758.
(12) Kawata, S.; Sun, H.-B.; Tanaka, T.; Takada, K. *Nature* **2001**, *412*, 697−698.
(13) Olson, C. E.; Previte, M. J.; Fourkas, J. T. *Nat. Mater.* **2002**, *1*, 225−228.
(14) Basu, S.; Campagnola, P. J. *Biomacromolecules* **2004**, *5*, 572−579.
(15) Olveczky, B. P.; Verkman, A. S. *Biophys. J.* **1998**, *74*, 2722−2730.

(16) Periasamy, N.; Verkman, A. S. *Biophys. J.* **1998**, *75*, 557−567.
(17) Seksek, O.; Biwersi, J.; Verkman, A. S. *J. Cell Biol.* **1997**, *138*, 131−142.
(18) Wachsmuth, M.; Waldeck, W.; Langowski, J. *J. Mol. Biol.* **2000**, *298*, 677−689.
(19) Wachsmuth, M.; Weidemann, T.; Muller, G.; Hoffmann-Rohrer, U. W.; Knoch, T. A.; Waldeck, W.; Langowski, J. *Biophys. J.* **2003**, *84*, 3353−3363.
(20) Feder, T. J.; Brust-Mascher, I.; Slattery, J. P.; Baird, B.; Webb, W. W. *Biophys. J.* **1996**, *70*, 2767−2773.
(21) Saxton, M. *Biophys. J.* **1994**, *66*, 394−401.
(22) Saxton, M. J. *Biophys. J.* **1996**, *70*, 1250−1262.
(23) Sridhar, M.; Basu, S.; Scranton, V. L.; Campagnola, P. J. *Rev. Sci. Instr.* **2003**, *74*, 3474−3477.
(24) Li, M. Y.; Cline, C. S.; Koker, E. B.; Carmichael, H. H.; Chignell, C. F.; Bilski, P. *Photochem. Photobiol.* **2001**, *74*, 760−764.
(25) Balasubramanian, D.; Du, X.; Zigler, J. S. J. *Photochem. Photobiol.* **1990**, *52*, 761−768.
(26) Foote, C. S. In *Free Radicals in Biology*; Pryor, W. A., Ed.; Academic Press: New York, 1976; Vol. 2, pp 85−134.
(27) Koppel, D. E. *Biophys. J.* **1979**, *28*, 281−291.
(28) Kubitscheck, U.; Wedekind, P.; Peters, K. *J. Microsc.* **1998**, *192*, 126−138.
(29) Bevington, P. R.; Robinson, D. K. *Data Reduction and Error Analysis for the Physical Sciences, 2nd edition*; McGraw-Hill Inc.: New York, 1992.
(30) Campagnola, P. J.; R., H. A.; Delguidas, D.; Epling, G. A.; Pitts, J. D.; Goodman, S. L. *Macromolecules* **2000**, *33*, 1511−1513.
(31) Soeller, C.; Cannell, M. B. *Pflugers Arch-Eur. J. Physiol.* **1996**, *432*, 555−561.
(32) Dunn, A. K.; Wallace, V. P.; Coleno, M.; Berns, M. W.; Tromberg, B. J. *Appl. Opt.* **2000**, *39*, 1194−1201.
(33) Hell, S. W.; Stelzer, E. H. K. *Opt. Comm.* **1992**, *93*, 277−282.
(34) Gu, M.; Sheppard, C. J. R. *J. Microsc.* **1995**, *177*, 128−137.
(35) Leach, J. B.; Bivens, K. A.; Jr., C. W. P.; Schmidt, C. E. *Biotech. Bioeng.* **2003**, 578−589.
(36) Bowen, W. R.; Williams, P. M. *Biotech. Bioeng.* **1996**, *50*, 125−135.
(37) Van Keuren, E.; Schrof, W. *Macromolecules* **2003**, *36*, 5002−5007.
(38) Lenart, P.; Rabut, G.; Daigle, N.; Hand, A. R.; Terasaki, M.; Ellenberg, J. *J. Cell Biol.* **2003**, *160*, 1055−1068.
(39) Saxton, M. J. *Biophys. J.* **2001**, *81*, 2226−2240.
(40) Popov, S.; Poo, M. M. *J. Neurosci.* **1992**, *12*, 77−85.
(41) Gilbert, D. L.; Kim, S. W. *J. Biomed. Mater. Res.* **1990**, *24*, 1221−1239.
(42) Tsunomori, F.; Ushiki, H. *Phys. Lett. A* **1999**, *258*, 171−176.
(43) Kim, J.; Somorjai, G. A. *J. Am. Chem. Soc.* **2003**, *125*, 3150−3158.

BM049707U